Journal Pre-proof

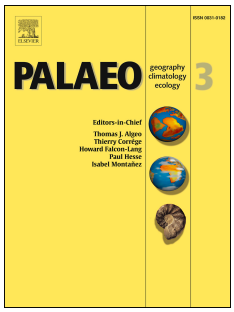

Vegetation succession and climate change across the Plio-Pleistocene transition in eastern Azerbaijan, central Eurasia (2.77–2.45 Ma)

Thomas M. Hoyle, Suzanne A.G. Leroy, Lourdes López-Merino, Daniel P. Miggins, Anthony A.P. Koppers

PII: S0031-0182(18)30876-9

DOI: https://doi.org/10.1016/j.palaeo.2019.109386

Reference: PALAEO 109386

To appear in: *Palaeogeography, Palaeoclimatology, Palaeoecology*

Received Date: 20 October 2018

Revised Date: 12 September 2019

Accepted Date: 23 September 2019

Please cite this article as: Hoyle, T.M., Leroy, S.A.G., López-Merino, L., Miggins, D.P., Koppers, A.A.P., Vegetation succession and climate change across the Plio-Pleistocene transition in eastern Azerbaijan, central Eurasia (2.77–2.45 Ma), *Palaeogeography, Palaeoclimatology, Palaeoecology*, https://doi.org/10.1016/j.palaeo.2019.109386.

Vegetation succession and climate change across the Plio-Pleistocene transition in eastern Azerbaijan, central Eurasia (2.77–2.45 Ma)

Thomas M. Hoyle [1, *], Suzanne A. G. Leroy[2], Lourdes López-Merino[3], Daniel P. Miggins[4], Anthony A.P. Koppers[4]

[1] Department of Earth Sciences, Utrecht University, Budapestlaan 17, Utrecht 3584 CD, The Netherlands

[2] Aix Marseille Univ, CNRS, Minist Culture, LAMPEA, UMR 7269, 5 rue du Château de l'Horloge, 13094, Aix-en-Provence, France

[3] Department of Geography, Geology and the Environment, Kingston University, Penrhyn Road, Kingston upon Thames, Surrey, KT1 2EE, UK

[4] OSU $^{40}Ar/^{39}Ar$ Geochronology Laboratory, Oregon State University, Corvallis, Oregon, 97331-5503, USA

*Corresponding author e-mail: Thomas.m.hoyle@gmail.com

Key words: Palynology; taphonomy; Milankovitch forcing; Obliquity; Caspian Sea; $^{40}Ar/^{39}Ar$ geochronology

Abstract

The Plio-Pleistocene transition marked a key moment in global climate history, characterised by the onset of major glaciations in the Northern Hemisphere. The palaeoenvironmental history of the Plio-Pleistocene transition is not well known for the Caspian Sea region, despite its importance for global climate dynamics. Here we present an independently $^{40}Ar/^{39}Ar$ dated, high-resolution terrestrial palynological record spanning the Plio-Pleistocene boundary based on a lacustrine-marine sedimentary sequence from eastern Azerbaijan. Despite complex pollen transport pathways and the proximity of closely stacked mountain vegetation belts in the Greater and Lesser Caucasus, the record shows that regional vegetation responded to Milankovitch forced glacial-interglacial cycles, tentatively correlated with global climatic records spanning MIS G8 to 98 (~2.77–2.45 Ma). The persistence of mesophilous forests during glacial times indicates that some settings in the South Caspian Basin acted as glacial refugia, and that vegetation response to glaciations was muted by increased moisture availability, linked to Caspian transgression. The palynological record shows a relationship with global $\delta^{18}O$ stacks and specifically to the obliquity record. We anticipate that precise correlation with the global climatostratigraphic timescale will allow better understanding of the nature and timing of important transgressive events in the Caspian Sea and their relevance on a global scale.

1. Introduction

The Pliocene-Pleistocene transition (~2.7–2.5 Ma) was a key episode in Earth's climate history when large, permanent ice sheets began to form in the Northern Hemisphere (Bartoli et al., 2005). This climatic cooling had a significant impact on Earth systems, including vegetation (Donders et al., 2018; Leroy and Dupont, 1994; Vallé et al., 2014). However, very little information is available about vegetation trends across the Plio-Pleistocene in central Eurasia, including in the Caucasus, which is a biodiversity hotspot in the present-day (Connor and Kvavadze, 2009). A variety of vegetation has been recorded in the Caspian Sea region as occurring during the late Pliocene and early Pleistocene (Figure 1), including deciduous and coniferous forests in the Mineral'nyye Vody, Tersko-Sunzhensky and Dagestan foothills regions (north-western margins of the Caspian) (Naidina and Richards, 2016). On the eastern shores of the Caspian Sea, much of what is now Turkmenistan was covered with tropical savannah from the Paleocene-Lower Oligocene onwards, with sparse vegetation and few trees (Atamuradov, 1994). The aridification trend continued through the late Pliocene and into the Pleistocene, by which time the area had developed a highly xerophytic flora, including species of Asteraceae, Poaceae and Amaranthaceae (Kurbanov, 1994). Evidence of the flora of the Iranian shore of the Caspian across the Plio-Pleistocene transition is comparatively scarce, although Akhani et al. (2010) suggest that the climate was warmer than today and that at least part of Iran was covered by steppe vegetation during that time interval.

In the Precaspian and fore-Ural region, the total number of floristic taxa decreased across the Plio-Pleistocene transition, and coniferous taiga forests

dominated by *Pinus* and *Picea* along with some deciduous elements, spread towards the south (Danukalova et al., 2009). Landscapes in parts of the Bashkortostan region (Figure 1) were characterised by dwarf birch and steppe assemblages, as well as coniferous forests, eventually giving way to steppes of *Artemisia*, Amaranthaceae and Poaceae in the early Pleistocene (Danukalova et al., 2009). However, no detailed palynological record has ever been published covering vegetation change over the Plio-Pleistocene transition in the region between the Greater and Lesser Caucasus. In particular, no record for this region and time period has been used to determine climate variation on orbital timescales (tens of thousands of years). Given the complex physiographic conditions – including the rising Caucasus Mountains – as well as the presence of Tertiary relicts and floristic taxonomical assemblages that may not have current analogues, the study area presents a challenging and atypical set of circumstances in terms of past vegetation and climate reconstruction. It is nonetheless one that has never (to our knowledge) been investigated at Milankovitch-scale resolution.

In this new study, we present an independently dated, high-resolution terrestrial palynological record from the Caucasus region recovered from a Caspian Sea sedimentary archive in eastern Azerbaijan (Figure 1). We aim to obtain a robust landscape reconstruction across the Plio-Pleistocene transition at the resolution of the Milankovitch cycles. In-so-doing we have the objective of deciphering long-term vegetation and landscape changes which can be linked to a regional climatic framework.

2. Materials and methods

2.1 Lithostratigraphical setting

The Lokbatan section crops out ~10 km west of Baku, Azerbaijan, and exposes the top of a north-south trending anticline. The section lies to the west of the road between Lokbatan and Qobu (N 40° 20’ 43”, E 49° 44’ 35”) and exposes sediments of the uppermost Productive Series (Pliocene), Akchagylian (late Pliocene and early Pleistocene) and basal Apsheronian (early Pleistocene). Lokbatan section sediments comprise homogenous blue-grey clayey silts. Strata strike north-south and dip ~45° towards the east. This part of the section is known as the Akchagylian ash interval, due to the presence of a series of intercalated layers of volcanic tuff. The section presented here was logged and equated with previous studies (Van Baak et al., 2013; Vincent et al., 2010) for ease of correlation and was logged and sampled at exactly the same exposure as Van Baak et al. (2013). The interval represents a distal pro-delta to offshore depositional setting and is the same as the marine-influenced interval 528–541 m of Van Baak et al. (2013).

The ash-bearing section formed a ~12.4 m thick unit of homogenous dark bluish-greenish grey (Gley 2, 4/1) clayey silt (Figure 2). Faint lamination was noted in the clays between 528.8 m and 541.5 m, without other sedimentary structures or indicators of bioturbation. Ostracod valves were observed very occasionally, but no burrows were seen in the studied interval during sampling. Interspersed through the interval from 528.8 m to 541.2 m were variably white-grey (2.5Y 8/1 to 6/1) ash layers with biotite mica flakes.

The thickest ash layers (>0.1 m) occurred at 528.8 m (ash 1), 532.0 m (ash 2), 532.6 m (ash 3), 533.0 m (ash 4), 534.4 m (ash 5), 537.8 m (ash 7), 540.2 m (ash 8) and 541.2 m (ash 9). A sequence of thinner (<0.01 m) ash layers was observed at ~534.8–536.2 m, which is referred to as ash complex 6 (Figure 2). Some of the

ashes appeared orange and weathered. Ashes 1, 2, 3, 4, 5, 7 and 9 were sampled for argon dating with the aim of building an accurate age-depth model for the studied interval.

2.2 $^{40}Ar/^{39}Ar$ analytical methods

The seven selected ash samples were processed for biotite, the only datable phase present in each of the ashes. Each sample was crushed into the smallest pieces and placed in large pyrex beakers and filled with cold tap water. The procedure for liberating the biotites and other crystals from the clay-rich ashes is to ultrasonically break down the clays over 2 to 5 days. The biotites where then dried in a drying over at 55 ^{o}C. Once the biotites were concentrated, they were either magnetically separated from the remaining material after the ultrasonic bath treatment or they were concentrated using a method called paper shaking. All biotite splits were picked to a purity of >99% using a binocular microscope.

Seven new biotite ages were obtained by means of the $^{40}Ar/^{39}Ar$ laser total fusion method using the ARGUS-VI mass spectrometer. The biotites were irradiated in OSU irradiation package 16-OSU-01 for 6 hours in the Oregon State University TRIGA reactor in the CLICIT position, along with the Fish Canyon Tuff sanidine (FCT-2; 28.201 ± 0.023 Ma, 1σ) flux monitor (Kuiper et al., 2008). Individual J-values for each sample were calculated by parabolic extrapolation of the measured flux gradient against irradiation height and typically give 0.2-0.3% uncertainties (1σ). The $^{40}Ar/^{39}Ar$ incremental heating age determinations were performed on a multi-collector ARGUS-VI mass spectrometer at Oregon State University that has 5 Faraday collectors (all fitted with 1012 Ohm resistors) and 1 ion-counting CuBe electron multiplier (located in a position next to the lowest mass Faraday collector). This

allows us to measure all argon isotopes simultaneously, with mass 36 on the multiplier and masses 37 through 40 on the four adjacent Faradays. This configuration provides the advantages of running in a full multi-collector mode while measuring the lowest peak (on mass 36) on the highly sensitive electron multiplier (which has an extremely low dark-noise and a very high peak/noise ratio). Irradiated samples were loaded into Cu-planchettes in an ultra-high vacuum sample chamber where each biotite crystal was heated until it was fused (total fusion) by scanning a defocused 25 W CO_2 laser beam in pre-set patterns across the sample, in order to release the argon evenly. After heating, reactive gases were cleaned up using an SAES Zr-Al ST101 getter operated at 400°C for ~10 minutes and two SAES Fe-V-Zr ST172 getters operated at 200°C and room temperature, respectively. All ages were calculated using the corrected Steiger and Jäger (1977) decay constant of 5.530 ± 0.097 x 10-10 1/yr (2σ) as reported by Min et al. (2000). For all other constants used in the age calculations we refer to Table 2 in Koppers et al. (2003). All ages were derived using relative probability plots (Ideogram plots) that yielded a weighted mean age for one or more peaks. These Ideogram ages do not include the uncertainty in the J-value. Incremental heating plateau ages and isochron ages (if calculated) were calculated as weighted means with 1/σ2 as weighting factor (Taylor, 1997) and as YORK2 least-square fits with correlated errors (York, 1969) using the ArArCALC v2.6.2 software from Koppers (2002) available from the http://earthref.org/ArArCALC/ website.

Age-depth relationships were modelled using the Clam 2.2 plug-in for R version 3.3.3 (Blaauw, 2010; R core team, 2017).

2.3 Palynological analysis

Sixty-four sediment samples of ~5 cm^3 were processed for palynological analysis at Brunel University London using cold hydrochloric acid (HCl, 35%) to remove carbonates, and cold hydrofluoric acid (HF, 60%) and HCl again to dissolve silicates and to prevent the formation of silicate gels respectively. Density separation using sodium polytungstate (SPT, specific gravity of 2.4) was used to remove residual minerals. Finally, residues were sieved through disposable nylon meshes (125 and 10 µm) and the 10–125 µm fraction was retrieved. The final residues were mounted on slides using glycerol. *Lycopodium clavatum* spores (batch number: 3862) were added to each sample prior to processing to allow calculation of concentrations.

Counting was carried out at magnifications of × 400 and × 1000 using a binocular transmitted light microscope. Identifications were made aided by reference texts (Menke, 1976; Moore and Webb, 1978; Reille, 1992) and the Brunel University London reference collection. Counts of over 300 terrestrial pollen grains per sample were obtained in most samples, although lower counts were reached in some levels with poor preservation. Palynological percentages were calculated on the terrestrial pollen sum, which includes the sum of all tree (including Pinaceae), shrub and upland herb pollen types. Pollen of obligate aquatic herbs as well as spores of ferns, reworked pollen, algal and fungal material were not included in the terrestrial pollen sum, but are expressed as a percentage of it. The palynological diagram was plotted using Psimpoll 4.27 (Bennett, 2008), with all taxa except *Pinus* plotted after recalculation of percentages excluding *Pinus*.

The zonation of the palynological record was performed using stratigraphically constrained cluster analysis by sum of squares (CONISS) after square-root transformation on all taxa exceeding 5% of the terrestrial pollen sum, using Psimpoll 4.27 (Bennett, 2008). The ratio of arboreal pollen (AP = trees and shrubs) and non-

arboreal pollen (NAP = herbs) was calculated by dividing the sum percentage of all tree and shrub taxa by the sum percentage of all herbaceous taxa (= AP/NAP ratio). This ratio presents an indication of how densely forested the contemporary landscape was, and by extension, is linked with temperature and moisture availability (higher ratio = warmer and wetter) (Li et al., 2010).

3. Results

3.1 $^{40}Ar/^{39}Ar$ geochronology and age-depth model

A summary of the results obtained from the seven volcanic ash layers dated is given in Table 1. Ideogram plots are presented in Figure 3 and additional information, including raw data, is given in the supplementary material to this paper. Weighted mean ages obtained were: 2.73 ± 0.09 Ma (ash 1), 2.68 ± 0.03 (ash 2), 2.67 ± 0.02 Ma (ash 3), 2.66 ± 0.02 Ma (ash 4), 2.60 ± 0.03 (ash 5), 2.73 ± 0.05 Ma (ash 7) and 2.66 ± 0.05 Ma (ash 9). All ages are shown at 2 σ.

Two of the dates (ash 7 and ash 9) were not incorporated into the age-depth model as they overlap in age with dates from lower stratigraphic levels (Figure 2). For these dates to be correct would require large-scale displacement/slumping or complete inversion in the upper part of the section, neither of which was apparent during careful re-inspection of the sampling site. It is more likely that the upper ashes may have sampled similar populations of biotite as the lower ashes (perhaps due to crystallisation in the magma chamber long prior to eruption) or that ashes 7 and 9 could have more excess argon than the lower levels, giving an artificially older age. It is also possible that some weathered cortex that was not removed during sampling

of the top two ashes could have affected the laboratory analyses. This aspect of the age-depth model could therefore lead to uncertainty in correlation with global cycles. As such, the five dates that provided coherent stratigraphical results were used to build an age-depth model (Figure 2). The chosen model is a simple linear regression, assuming constant accumulation rates for the reconstructed period (2.77–2.45 Ma). Model output is provided in supplementary material.

3.2 Terrestrial palynology

The palynological record of the section presented here (Figures 4 [trees], 5 [shrubs and herbs] and 6 [aquatic vegetation, ferns, NPP and reworked], with full dataset included in supplementary material) includes *Pinus* throughout the pollen record, sporadically showing large peaks (Figure 4). Other conifers such as *Picea*, *Cedrus* and *Abies* (as well as undifferentiated bisaccate grains) also have a consistent presence across the entire record but with lower representations. Temperate forest elements such as *Ulmus-Zelkova*, *Quercus*, *Carpinus* and *Alnus* are also well represented. Overall, the described AP component shows a seesaw pattern opposite to the one shown by the NAP component, especially by Amaranthaceae, Asteraceae (mostly Asteroideae) and *Artemisia* (Figure 5). Changes in the percentages of these taxa allowed the detection of nine pollen assemblage zones (PAZs) that were obtained by cluster analysis, numbered from the base of the section upwards (Figure 6).

PAZ-1 (528.3–530.2 m, 10 samples) has consistent representation of coniferous taxa, primarily *Pinus* (~27-7%), but also *Picea* (~8-2%) and *Cedrus* (~14-2%). Other AP elements with important representation are *Ulmus-Zelkova* (~18-3%), *Quercus* (~9-1%), *Carpinus* (<4%) and *Alnus* (~6-1%). On the other hand,

Amaranthaceae (~22-9%) and *Artemisia* (~19-4%) are the more abundant NAP taxa. The levels of reworking are elevated relative to most of the rest of the sequence. Peaks in fungal remains (fungal spores, hyphae and fruiting bodies) occur in the upper part of the zone.

PAZ-2 (530.2–532.4 m, 12 samples) shows increase in temperate forest elements, especially *Quercus* (~17-3%) but also *Alnus* (~13-3%), *Carpinus* (<5%) and *Ulmus-Zelkova* (~17-1%), coeval with a decrease in the representation of coniferous taxa (*Pinus*: ~13-2%). Among the NAP taxa, *Artemisia* (~35-5%) displays higher percentages than Amaranthaceae (~17-8%). Fungal material is present consistently.

In PAZ-3 (532.4–533.6 m, 6 samples), *Pinus* (~55-8%) is the main AP taxon together with *Quercus* (~17-1%), *Alnus* (<9%) and *Ulmus-Zelkova* (<8%). Among the NAP taxa, Amaranthaceae (~26-7%) and Asteroideae (~13-3%) become abundant together with increases in the values of Poaceae (~11-1%), Caryophyllaceae (<6%) and Cichorioideae (<5%), while *Artemisia* percentages are low (<7%). A large peak in reworking is noted towards the top of the zone, coincident with the first *Ephedra* peak (~6-0.5%) of the sequence.

Pinus (~9-1%) percentages decrease again in PAZ-4 (533.6–534.6 m, 5 samples), while *Cedrus* (~18-0.3%) and *Alnus* (~18-2%) present increasing values, and *Ulmus-Zelkova* (~18-8%) is the best represented AP pollen type. Amaranthaceae (~26-6%) continues having high values, while *Artemisia* (~22-4%) percentages increase and are high along the entire zone.

The AP component in PAZ-5 (534.6–535.2 m, 3 samples) sees a drop in the values of *Ulmus-Zelkova* (~6-1%), *Cedrus* (<2%) and *Alnus* (<1%), and a new increase in those of *Pinus* (~40-12%) and *Abies* (~5-2%). The NAP component is

dominated by the high values for Amaranthaceae (~25-7%) and Poaceae (~20-6%) along with the decreased percentages of *Artemisia* (~11-2%). This zone records a second peak in *Ephedra* (~8-1%).

PAZ-6 (535.2–536.2 m, 5 samples) shows a decrease in *Pinus* values (~20-3%) and increases in the representation of other AP taxa such as *Ulmus-Zelkova* (~22-5%), *Alnus* (<10%), *Tsuga* (~6-1%) and *Cedrus* (~20-1%). Among the NAP component, Amaranthaceae (~13-3%) and Poaceae (~12-3%) show decreasing values, while the percentages of *Artemisia* (~12-6%) slightly increase.

In PAZ-7 (536.2–537 m, 4 samples) the percentages of *Pinus* further decrease (~5-2%) as well as those of *Cedrus* (~6-2%) and *Tsuga* (<1%). Although the presence of *Ulmus-Zelkova* decreases (~15-5%) in comparison with the previous zone, the percentages are still important. *Quercus* (~11-10%) and *Alnus* (~10-2%) are other AP elements with significant values. Among the NAP taxa, Amaranthaceae (~17-9%) continues with the same level of presence, while *Artemisia* (~32-9%) values increase and Poaceae (~8-1%) values decrease. Fungal material becomes more common in PAZ-7.

PAZ-8 (537–539.6 m, 12 samples) shows seesaw patterns in the percentages of AP and NAP taxa. On the one hand, *Pinus* (~40-2%), *Quercus* (<22%), *Ulmus-Zelkova* (<9%), *Cedrus* (<10%), *Picea* (<6%), *Abies* (<5%), *Alnus* (<6%) and Cupressaceae (<3%) are the best represented AP taxa. On the other hand, *Artemisia* (<39%), Amaranthaceae (~25-2%), Asteroideae (~10-2%), Cichorioideae (<12%), Poaceae (~27-2%) and Caryophyllaceae (<6%) are the best represented NAP taxa. Sporadic peaks of fungal material and reworking occur throughout PAZ-8.

Two samples presented palynologically barren levels between PAZ-8 and PAZ-9.

PAZ-9 (539.6–541.1 m, 5 samples) shows high representation of *Ulmus-Zelkova* (~24-5%) with increasing values of *Alnus* (~15-1%), *Carpinus* (~4-1%) and *Corylus* (~3-1%), and decreasing values of *Quercus* (~1-6%), *Pinus* (~16-4%) and other coniferous such as *Cedrus* (<1%), *Abies* (<3%) and Cupressaceae (~2-1%). *Artemisia* (~50-7%) and Amaranthaceae (~20-10%) are the best represented NAP taxa, while Asteroideae (~8-2%), Cichorioideae (~4-1%) and Poaceae (~8-2%) present decreasing values. Refer to supplementary material for the complete dataset.

4. Discussion

4.1 Geochronological framework

The linear regression age-depth model using the new $^{40}Ar/^{39}Ar$ spectrometry data suggests that the Akchagylian ash interval spans from ~2.77 to ~2.45 Ma, covering a period of ~320 ka (Figure 2). The age-depth model is the most consistent in the middle part of the record, where the density of age determinations is high and the uncertainties for the $^{40}Ar/^{39}Ar$ ages are small (<0.03 Ma). The model shows large uncertainty at the base of the record (0.09 Ma) and at the top of the sequence, where no radiometric data could be incorporated (Figure 2).

Van Baak et al. (2013) documented two different radiometric ages for the ashes in the Akchagylian of the Lokbatan section; a fission track age of 3.34 ± 0.35 Ma (Chumakov et al., 1988) and 2.6–2.4 Ma, referred to Groves et al. (1996). However, Chumakov et al. (1992) later cautioned that these fission track dates should be taken as preliminary, to be tested in future. As such, our dates are consistent with one of the two potential ages presented by Van Baak et al. (2013).

Furthermore, the interpreted stratigraphic correlation of Van Baak et al. (2013) has now been superseded by new $^{40}Ar/^{39}Ar$ ages for the Akchagylian from the nearby Jeirankechmez outcrop, Azerbaijan (Van Baak et al., 2019). Given the complete agreement in ages provided by Van Baak et al. (2019) with those presented in this paper for the Lokbatan outcrop, there is reason to be confident in the new ages and to give them priority over previous determinations. These ages support the "short Akchagylian" scenario presented by Krijgsman et al. (2019).

Average sedimentation rate determined using our age-depth model is ~0.04 m/ka, which is much lower than that of the underlying Surakhany Suite that has been estimated at ~1.0 m/ka (Van Baak, 2015; Van Baak et al., 2013). Sedimentation rates at Lokbatan also increase somewhere in the interval above 545 m, to 0.41 m/ka during the Olduvai chron (Van Baak et al., 2013). This means that the sedimentation rate in the ash interval is an order of magnitude lower than during the Olduvai chron. Given that 160 m stratigraphic thickness exists between the top of the ash interval and the base of the Olduvai chron, we suggest that sedimentation rates during the majority of this interval must have been more similar to those in Olduvai chron than those in the ash interval. This is especially the case if a hiatus exists at 660 m (Van Baak et al., 2013).

This pattern of sedimentation rates is consistent with the Akchagylian representing a regionally extensive condensed section (Abdullayev et al., 2012). One potential explanation for this pattern is that sedimentation rate increased due to enhanced physical weathering during and after some of the earliest major glaciations (MIS 100-98-96). It is possible to suggest a tentative age-depth relationship up section from the $^{40}Ar/^{39}Ar$ dated interval by assuming constant sedimentation rate between the top of the ash interval and the base of the Olduvai chron.

The ejection site of the ashes at Lokbatan is not known. However, they are time-equivalent with major volcanic activity in the Lesser Caucasus, including formation of major plateau basalts in southern Georgia (~2.9-1.9 Ma) and the first major phase of activity of the Aragats volcanic centre in Armenia (2.5 ± 0.2 Ma) (Chernyshev et al., 2002). It is possible that one of these Caucasian volcanic centres was the source for the Akchagylian ashes.

4.2 Taphonomic considerations

The palynological record shows relatively homogeneous assemblages with a diverse range of taxa present ubiquitously (Figures 4, 5 and 6). However, the variable record of reworked material indicates that palynological assemblages could be influenced by taphonomic issues, such as differential preservation and pollen transport mechanisms (Hoyle et al., 2018). Once these topics are addressed, it is possible to correlate vegetation dynamics in eastern Transcaucasia with the global climate record across the Plio-Pleistocene transition (Richards et al., 2018; Van Baak, 2015; Van Baak et al., 2019).

In the present day, the area between the Greater and Lesser Caucasus contains a large range of relief, meaning that a huge diversity of habitats is represented across relatively small areas, e.g. steppe, forest, semi-desert, coastal, floodplain and wetland. The Volga is the main source of water (>80%) for the Caspian Sea (Arpe et al., 2018). However, the palaeo-delta and the contemporaneous northern coastline lay over 1000 km north of the study location (north of the latitude of Volgograd) during the Plio-Pleistocene transition (Popov et al., 2006). Data from palynological case-studies offshore N-W Africa, in the Gulf of Guinea and in the western Mediterranean, suggest that the majority of palynomorphs

fall from suspension within a short distance of river mouths (often due to incorporation in faecal pellets) and that wind transport is more important in pollen distribution (Beaudouin et al., 2007; Dupont and Agwu, 1991; Hooghiemstra et al., 2006). Despite surface currents, we therefore consider it unlikely that the northern rivers were a major contributor to the pollen signal of the Akchagylian sediments at Lokbatan.

Rivers in the present Kura-Araz (respectively also known as Mtkvari and Arax) drainage cut through multiple vegetation belts, including from Mediterranean, attenuated sub-desert and cold axeric climates. The modern Kura and tributaries alone flow through shrub and tree pseudo-steppes under dry climate, tall grass steppes under temperate and cold temperate climate, plateaux and sub-mountain steppes, deciduous and semi-evergreen oak forest belt formations, dry sub-alpine belt, western wet mountain belt, western dry mountain belt, western wet sub-mountain belt and western dry sub-mountain belt (Lalande, 1968). Also taking the Araz catchment into account adds sub-humid Mediterranean belt and oak and juniper belt formations.

This vast array of vegetation types within the catchment of the probable feeding river systems has the potential to deposit a diverse yet relatively homogeneous pollen assemblage with many environments represented throughout the sequence. It is also likely that various coastal saline-influenced wetlands and swamps would have existed in the past, just as in the present day, which were controlled by topography and edaphic circumstances rather than by climate. Assuming that the late Pliocene and early Pleistocene Kura Valley was also diverse (which the pollen assemblages support), changes in assemblage composition probably represent changes in the distribution of this vegetation through time, by

vertical movement of vegetation belts, driven by changes in precipitation and temperature.

In the present day, winds in the Lokbatan locality are predominantly from the east during the winter and from the north during the summer (Ibrayev et al., 2010). If similar circumstances existed around the Plio-Pleistocene transition, then this could bring pollen from the regions of Turkmenistan, Kazakhstan and potentially also from the Russian platform. Even if we cannot be certain of the directions of prevailing winds in the past, it is plausible that pollen from the xerophytic vegetation from the east and the taiga and steppe from the north could have been introduced to the depositional site.

4.3 Correlating the pollen successions with the global $\partial^{18}O$ record

The detection of glacial-interglacial cycles in the pollen record thanks to changes in the AP/NAP ratio allows correlation of the linear regression age-depth model obtained using the $^{40}Ar/^{39}Ar$ dates from the sedimentary record with global climatic changes. We use the marine oxygen isotope stages of Lisiecki and Raymo (2005) as well as the obliquity curve of Laskar et al. (2004) to find common patterns of change (Figure 2).

The clearest relationships with global climate are apparent where the age-depth model is strongest (2.68 to 2.60 Ma, top of PAZ-2, PAZ-3 to PAZ-5). In this interval, lower AP/NAP ratios in PAZ-3 and PAZ-5 are clearly related with reductions in temperate forest assemblages (*Quercus*, *Ulmus-Zelkova*, *Alnus*, Juglandaceae, etc.; Figure 4) and are accompanied by increases in *Ephedra* and Amaranthaceae, indicators of dry environments (Figure 5). In addition, the percentages of *Pinus* (plus bisaccates) also increase in PAZ-3 and PAZ-5, likely indicating colder conditions and

potentially a displacement of high-altitude pines to lower elevation belts. According to the linear regression age-depth model (Figure 2), both of these dry peaks correlate with obliquity minima (Laskar et al., 2004). Further, the associated $^{40}Ar/^{39}Ar$ date (2.60 ± 0.03 Ma at 534.40 m) allows correlation of the cold-dry vegetation signal in PAZ-5 with the only glacial period within error of the date: MIS 104 (2.614 to 2.595 Ma, Figure 7). The *Ephedra* peak in PAZ-3 also sits within range of an ash date (2.66 ± 0.02 Ma at 533.0 m), allowing correlation with MIS G2 (2.652 to 2.638 Ma, Figure 7).

Above this interval, the age-depth model has no dates, so correlations are more speculative. Based on the trend of the AP/NAP ratio, we tentatively correlate lower AP/NAP ratios in PAZ-7 to glacial episode MIS 102 (Figure 7). In addition, the following lower AP/NAP ratios in the middle of PAZ-8 and in the boundary of PAZ-8 and PAZ-9, the latter also including barren samples (Figure 7), could be linked to two of the first large glaciations of the Quaternary: MIS 100 (2.54 to 2.51 Ma) and MIS 98 (2.494 to 2.477 Ma) respectively. The intervening periods, where the representation of deciduous forests is relatively high and the AP/NAP ratios increase, are therefore linked to interglacial periods MIS 103, MIS 101 and MIS 99 respectively (Figure 7). The top sample, with increased representation of deciduous forest could represent climatic warming during MIS 97.

The glacial-interglacial correlation provided here calls for decreased sedimentation rate during MIS 100 and increased sedimentation rate during MIS 98. This latter phenomenon is consistent with the increased abundance of damaged and reworked grains at the top of PAZ-8 (Figure 6), and could be related with enhanced transport of clastic material into the basin, potentially by glacial outwash during the subsequent warming phase. This could also potentially explain the older dates

provided by Ash 9 and Ash 7, as enhanced reworking in the pollen in PAZ-8 could have been accompanied by clastic reworking from the older ash layers deposited in more proximal locations, however, this is purely speculative.

In the lower part of the sequence (PAZ-1 and PAZ-2), plotting samples according to the $^{40}Ar/^{39}Ar$ age-depth model does allow correlation of past vegetation patterns with climate, although with more caution. Small decreases in the AP/NAP ratios in the middle of PAZ-2 and the top of PAZ-1 are tentatively linked to MIS G4 and MIS G6 respectively. Although G5 is not strongly discernible from G6 and G4 in the global stack of Lisiecki and Raymo (2005) (MIS G5 presents the highest $\delta^{18}O$ values for all the interglacial periods covered by the sequence), the AP/NAP ratio (excluding *Pinus* and undifferentiated bisaccate grains) shows that clear changes in the vegetation occurred (Figure 7).

Apparent increase in sedimentation rate during MIS G3 and G2 (Figure 7) is due to the presence of three relatively thick volcanic ash layers (Ash 2, 3 and 4), which contribute a total thickness of 0.26 m despite representing near instantaneous deposition. As such, we correlate high AP/NAP ratios with G5 and G7 and low AP/NAP ratios with G4, G6 and potentially G8, although the relatively large uncertainty on the $^{40}Ar/^{39}Ar$ date near the base of the sequence (± 90,000 years in Ash 1) does not allow precise radiometric constraint.

Therefore, it seems that eight complete glacial-interglacial cycles are represented in the interval studied. As such, although changes in Transcaucasian vegetation appear to have been linked with global climate, they could also have been attenuated by regional alterations in moisture availability due to the large-scale transgression of the Caspian around the Plio-Pleistocene transition (Richards et al., 2018). In fact, it has been suggested that the size of the Caspian Sea can have

significant effects not only regionally, but can also impact atmospheric circulation on a global scale (Arpe et al., 2018). Given that the suggested transgression around the Plio-Pleistocene transition would have expanded the Caspian Sea surface area significantly, moisture transport from the Caspian Sea to the Kura depression by easterly winds could have been enhanced at this time (Arpe et al., 2018; Richards et al., 2018).

4.4 Vegetation cycles across the Plio-Pleistocene transition and glacial refugia

The chronological framework reconstructed for the section studied here seems to cover eight obliquity cycles, and the resolution of our palynological record allows for orbital correlation across most of this sequence. Despite the complications inherent in interpreting upland pollen data from marine environments, glacial-interglacial cycles are clearly picked out by variations in the AP/NAP ratio (Figure 7), reflecting broad changes in vegetation at a basin scale. AP elements are more dominant during interglacial periods, where climatic conditions were milder, while NAP elements are more abundant during glacial times, when cool climate hampered the development of extensive forests. However, thermophiles (e.g. *Quercus*, *Carpinus*, *Carya* and *Ulmus-Zelkova*) persisted during all the glacial phases covered by the Plio-Pleistocene section presented here, supporting the idea that Transcaucasia (= South Caucasus and lowlands) acted as a glacial refugium (Arpe et al., 2011; Leroy and Arpe, 2007)

On a regional scale, many temperate and Mediterranean taxa that still form a portion of the modern Transcaucasian flora were already present during the Plio-Pleistocene transition (e.g. *Populus*, *Ostrya*, *Fagus*, *Zelkova*, *Tilia*, *Pyrus*, *Ligustrum*, *Salix*, *Prunus*, *Acer*, *Quercus*, *Pterocarya*) (Nakhutsrishvili, 2013). Given the

494 persistence of these Mediterranean and temperate taxa through the Quaternary and
495 up to the present day, the Akchagylian flora may be considered to have significant
496 similarities to the modern one, at least in terms of taxonomic composition
497 (Grossheim, 1948; Nakhutsrishvili, 2013). However, the role of refugia is attested to
498 by the survival of other taxa (e.g. *Parrotia persica*, *Pterocarya fraxinifolia* and
499 *Zelkova carpinifolia*), which survived up to the present day, but only within locations
500 where suitable climatic conditions were maintained regionally due to their orographic
501 circumstances, forming a buffer against global climate change (Combourieu-Nebout
502 et al., 2015; Leroy and Arpe, 2007; Magri et al., 2017; Ramezani et al., 2008).
503 In combination with the presence of glacial refuges in the Caucasus, such
504 moderating effects (e.g. Arpe et al., 2011; Leroy and Arpe, 2007) could go some way
505 to explaining the continued presence (albeit with reduced representation) of
506 mesophillous forest assemblages during glacial period G6. It is feasible that the
507 transgressive event went some way to masking the effects of the G7-G6 transition by
508 moderating climatic parameters and potentially even increasing moisture availability
509 during the glacial episode.
510
511 ## 5. Conclusions
512
513 A well-dated ($^{40}Ar/^{39}Ar$ dates on volcanic ash layers), high-resolution palynological
514 record from Central Eurasia covering the Plio-Pleistocene transition has been
515 studied palynologically. The record of changes in the AP/NAP ratio has shown cyclic
516 fluctuations that can be linked with the global climatostratigraphic timescale for the
517 interval 2.77-2.45 Ma (MIS G8 to MIS 97) at the Lokbatan section, Azerbaijan. This
518 suggests that the pollen records obtained show variation on orbital timescales, likely

controlled by oscillations in obliquity. Changes in pollen assemblages, synthetised in the AP/NAP ratio, are interpreted as primarily due to climatically-controlled displacements of altitudinal vegetation belts in adjacent mountain ranges (Greater Caucasus, Lesser Caucasus and potentially also Talysh).

The palaeoenvironments presented here cover a period of time when the Caspian Sea temporarily became connected with the global oceans; an event that has significant implications for our understanding of Caspian lake level change and biodiversity modifications. We suggest that transgression and lake expansion during this period may even have had an effect on catchment climate, by making conditions milder during late Pliocene glacial episodes, potentially with a feedback on regional vegetation. Further palynological analyses, obtaining a detailed dinoflagellate cyst record, could confirm this hypothesis.

All supplementary material related to this paper is available at: https://doi.pangaea.de/10.1594/PANGAEA.905798

Acknowledgements

This work was funded by BP Exploration Operating Company Limited as a grant to SL. We are grateful to Timme Donders for helpful suggestions during the preparation of this manuscript. Francesca Sangiorgi, Arjen Grothe, Keith Richards, Chris van Baak, Wout Krijgsman, and Adele Bertini provided helpful comments during the thought process that preceded the publication of this work. Fieldwork benefitted from the help of Vusala Aghayeva, Shahnaz Mammadova and Elshan Abdullayev. Three

544 anonymous reviewers offered helpful comments that have contributed to the
545 improvement of the manuscript.

546

547 References

548

549 Abdullayev, N.R., Riley, G.W., Bowman, A.P., 2012. Regional Controls on Lacustrine
550 Sandstone Reservoirs: The Pliocene of the South Caspian Basin, in: Baganz,
551 O.W., Bartov, Y., Bohacs, K., Nummedal, D. (Eds.), Lacustrine Sandstone
552 Reservoirs and Hydrocarbon Systems. American Association of Petroleum
553 Geologists, pp. 71–98.
554 Akhani, H., Djamali, M., Ghorbanalizadeh, A., Ramezani, E., 2010. Plant biodiversity
555 of Hyrcanian relict forests, N Iran: an overview of the flora, vegetation,
556 palaeoecology and conservation. Pak. J. Bot., Spec. Issue (S.I. Ali Festschrift)
557 42, 231–258.
558 Arpe, K., Leroy, S.A.G., Mikolajewicz, U., 2011. A comparison of climate simulations
559 for the last glacial maximum with three different versions of the ECHAM model
560 and implications for summer-green tree refugia. Clim. Past 7, 91–114.
561 Arpe, K., Tsuang, B.J., Tseng, Y.H., Liu, X.Y., Leroy, S.A.G., 2018. Quantification of
562 climatic feedbacks on the Caspian Sea level variability and impacts from the
563 Caspian Sea on the large-scale atmospheric circulation. Theor. Appl. Climatol.
564 1–14.
565 Atamuradov, K.I., 1994. Paleogeography of Turkmenistan, in: Fet, V., Atamuradov,
566 K.I. (Eds.), Biogeography and Ecology of Turkmenistan. Monographiae
567 Biologicae, Vol 72. Springer, Dordrecht, Dordrecht, pp. 49–64.
568 Bartoli, G., Sarnthein, M., Weinelt, M., Erlenkeuser, H., Garbe-Schönberg, D., Lea,

D.W., 2005. Final closure of Panama and the onset of Northern Hemisphere glaciation. Earth Planet. Sci. Lett. 237, 33–44.

Beaudouin, C., Suc, J., Escarguel, G., Arnaud, M., Charmasson, S., 2007. The significance of pollen signal in present-day marine terrigenous sediments: The example of the Gulf of Lions (western Mediterranean Sea). Geobios 40, 159–172.

Bennett, K., 2008. Psimpoll and pscomb: www.chrono.qub.ac.uk/psimpoll/psimpoll.html.

Blaauw, M., 2010. Methods and code for “classical” age-modelling of radiocarbon sequences. Quat. Geochronol. 5, 512–518.

Chernyshev, I. V, Lebedev, V.A., Arakelyants, M.M., Jrbashyan, R., Ghukasyan, Y., 2002. Geochronology of the Aragats volcanic center, Armenia: Evidence from K-Ar dating. Dokl. Earth Sci. 384, 393–398.

Chumakov, I.S., Byzova, S.L., Ganzey, S.S., Arias, C., Bigazzi, G., Bonadonna, F.P., Hadler Neto, J.C., Norelli, P., 1992. Interlaboratory fission track dating of volcanic ash levels from eastern Paratethys. A mediterranean-paratethys correlation. Palaeogeogr. Palaeoclimatol. Palaeoecol. 95, 287–295.

Chumakov, I.S., Byzova, S.L., Ganzey, S.S., Mamedov, A.V., Alekserov, B.D., 1988. Radiometric scale of the late Cenozoic of Azerbaijan. Geol. Razved. Y Razrab. Neftegazov. Mestorozhdeniy, N2 4-7 (in Russian).

Combourieu-Nebout, N., Bertini, A., Russo-Ermolli, E., Peyron, O., Klotz, S., Montade, V., Fauquette, S., Allen, J., Fusco, F., Goring, S., Huntley, B., Joannin, S., Lebreton, V., Magri, D., Martinetto, E., Orain, R., Sadori, L., 2015. Climate changes in the central Mediterranean and Italian vegetation dynamics since the Pliocene. Rev. Palaeobot. Palynol. 218, 127–147.

Connor, S.E., Kvavadze, E. V, 2009. Modelling late Quaternary changes in plant distribution, vegetation and climate using pollen data from Georgia, Caucasus. J. Biogeogr. 36, 529–545.

Danukalova, G.A., Yakovlev, A., Kosintcev, P., Agadjanian, A., Alimbekova, L., Eremeev, A., Morozova, E., 2009. Quaternary fauna and flora of the Southern Urals region (Bashkortostan Republic). Quat. Int. 201, 13–24.

Donders, T.H., Van Helmond, N.A.G.M., Verreussel, R., Munsterman, D., Veen, J. Ten, Speijer, R.P., Weijers, J.W.H., Sangiorgi, F., Peterse, F., Reichart, G.J., Sinninghe Damsté, J.S., Lourens, L.J., Kuhlmann, G., Brinkhuis, H., 2018. Land-sea coupling of early Pleistocene glacial cycles in the southern North Sea exhibit dominant Northern Hemisphere forcing. Clim. Past 14, 397–411.

Dupont, L.M., Agwu, C.O.C., 1991. Environmental control of pollen grain distribution patterns in the Gulf of Guinea and offshore NW-Africa. Geol. Rundschau 80, 567–589.

Grossheim, A.A., 1948. Vegetational cover of the Caucasus, MOIP, Moscow.

Groves, J.R., Stein, J.A., Babazade, A., Koshkarly, R.O., Mamedova, D.N., 1996. Biostratigraphic and isotopic evidence for determining rates of rock accumulation within the productive series of eastern Azerbaijan, in: AAPG Symposium on Rapidly Subsiding Basins, Baku, Azerbaijan Republic.

Hooghiemstra, H., Lézine, A.M., Leroy, S.A.G., Dupont, L.M., Marret, F., 2006. Late Quaternary palynology in marine sediments: A synthesis of the understanding of pollen distribution patterns in the NW African setting. Quat. Int. 148, 29–44.

Hoyle, T.M., Leroy, S.A.G., López-merino, L., Richards, K., 2018. Using fluorescence microscopy to discern in situ from reworked palynomorphs in dynamic depositional environments — An example from sediments of the late Miocene to

early Pleistocene Caspian Sea. Rev. Palaeobot. Palynol. 256, 32–49.

Ibrayev, R.A., Özsoy, E., Schrum, C., Sur, H.İ., 2010. Seasonal variability of the Caspian Sea three-dimensional circulation, sea level and air-sea interaction. Ocean Sci. 6, 311–329.

Koppers, A.A.P., 2002. ArArCALC - software for 40Ar/39Ar age calculations. Comput. Geosci. 28, 605–619.

Koppers, A.A.P., Staudigel, H., Pringle, M.S., Wijbrans, J.R., 2003. Short-lived and discontinuous intraplate volcanism in the South Pacific: Hot spots or extensional volcanism? Geochemistry, Geophys. Geosystems 4, 1–49.

Krijgsman, W., Tesakov, A., Yanina, T.A., Lazarev, S., Danukalova, G., Van Baak, Christiaan G C, Agustí, J., Alçiçek, M.C., Aliyeva, E., Bista, D., Bruch, A.A., Büyükmeriç, Y., Bukhsianidze, M., Flecker, R., Frolov, P., Hoyle, T.M., Jorissen, E.L., Kirscher, U., Koriche, S.A., Kroonenberg, S.B., Lordkipanidze, D., Oms, O., Rausch, L., Singarayer, J., Stoica, M., Van de Velde, S., Titov, V. V, Wesselingh, F.P., Baak, C G C Van, Agustí, J., Alçiçek, M.C., Aliyeva, E., Bista, D., Bruch, A.A., Büyükmeriç, Y., Bukhsianidze, M., Kroonenberg, S.B., Lordkipanidze, D., Oms, O., Rausch, L., Singarayer, J., Stoica, M., 2019. Quaternary time scales for the Pontocaspian domain: interbasinal connectivity and faunal evolution. Earth-Science Rev. 188, 1–40.

Kuiper, K.F., Deino, A., Hilgen, F.J., Krijgsman, W., Renne, P.R., Wijbrans, J.R., 2008. Synchronizing Rock Clocks. Science 320, 500–504.

Kurbanov, D., 1994. Flora of Kopetdagh, in: Fet, V., Atamuradov, K.I. (Eds.), Biogeography and Ecology of Turkmenistan. Monographiae Biologicae, Vol 72. Springer, Dordrecht, pp. 105–128.

Lalande, P., 1968. Carte du Tapis Végétal de la Région Méditerranéenne, Feuille Est

(Vegetation Map of the Mediterranean Region, East Sheet).

Laskar, J., Robutel, P., Joutel, F., Gastineau, M., Correia, a. C.M., Levrard, B., 2004. A long-term numerical solution for the insolation quantities of the Earth. Astron. Astrophys. 428, 261–285.

Leroy, S.A.G., Arpe, K., 2007. Glacial refugia for summer-green trees in Europe and south-west Asia as proposed by ECHAM3 time-slice atmospheric model simulations. J. Biogeogr. 34, 2115–2128.

Leroy, S.A.G., Dupont, L.M., 1994. Development of vegetation and continental aridity in northwestern Africa during the Late Pliocene: the pollen record of ODP site 658. Palaeogeogr. Palaeoclimatol. Palaeoecol. 109, 295–316.

Li, F., Sun, J., Zhao, Y., Guo, X., Zhao, W., Zhang, K., 2010. Ecological significance of common pollen ratios: A review. Front. Earth Sci. China 4, 253–258.

Lisiecki, L.E., Raymo, M.E., 2005. A Pliocene-Pleistocene stack of 57 globally distributed benthic δ18O records. Paleoceanography 20, 1–17.

Magri, D., Di Rita, F., Aranbarri, J., Fletcher, W., 2017. Quaternary disappearance of tree taxa from Southern Europe: Timing and trends. Quat. Sci. Rev. 163, 23–55.

Menke, B., 1976. Pliozäne und ältestquartäre Sporen- und Pollenflora von Schleswig-Holstein. Geol. Jahrb. R. A 32, 1–196.

Min, K., Mundil, R., Renne, P.R., Ludwig, K.R., 2000. A test for systematic errors in 40Ar/39Ar geochronology through comparison with U/Pb analysis of a 1.1-Ga rhyolite. Geochim. Cosmochim. Acta 64, 73–98.

Moore, P.D., Webb, J.A., 1978. An Illustrated Guide to Pollen Analysis. Hodder and Stoughton, Sevenoaks.

Naidina, O.D., Richards, K., 2016. Pollen evidence for Late Pliocene - Early Pleistocene vegetation and climate change in the North Caucasus, North-

669 Western Caspian Region. Quat. Int. 409, 50–60.
670 Nakhutsrishvili, G., 2013. The Vegetation of Georgia (South Caucasus), 2nd ed.
671 Springer, Berlin Heidelberg.
672 Popov, S. V, Shcherba, I.G., Ilyina, L.B., Nevesskaya, L.A., Paramonova, N.P.,
673 Khondkarian, S.O., Magyar, I., 2006. Late Miocene to Pliocene
674 palaeogeography of the Paratethys and its relation to the Mediterranean.
675 Palaeogeogr. Palaeoclimatol. Palaeoecol. 238, 91–106.
676 R core team, 2017. R: A language and environment for statistical computing.
677 Ramezani, E., Marvie Mohadjer, M.R., Knapp, H.-D., Ahmadi, H., Joosten, H., 2008.
678 The late-Holocene vegetation history of the Central Caspian (Hyrcanian) forests
679 of northern Iran. The Holocene 18, 307–321.
680 Reille, M., 1992. Pollen et spores d Europe et d Afrique du nord. Laboratoire de
681 Botanique Historique et Palynologie, Marseille.
682 Richards, K., Van Baak, C.G.C., Athersuch, J., Hoyle, T.M., Stoica, M., Austin,
683 W.E.N., Cage, A.G., Wonders, A.A.H., Marret, F., Pinnington, C.A., 2018.
684 Palynology and micropalaeontology of the Pliocene - Pleistocene transition in
685 outcrop from the western Caspian Sea, Azerbaijan: Potential links with the
686 Mediterranean, Black Sea and the Arctic Ocean? Palaeogeogr. Palaeoclimatol.
687 Palaeoecol. 511, 119–143.
688 Steiger, R.H., Jäger, E., 1977. Subcommission on geochronology: Convention on the
689 use of decay constants in geo- and cosmochronology. Earth Planet. Sci. Lett.
690 36, 359–362.
691 Taylor, J., 1997. Introduction to Error Analysis: The Study of Uncertainties in
692 Physical Measurements, 2nd ed. University Science Books, Mill Valley,
693 California.

694 Vallé, F., Dupont, L.M., Leroy, S.A.G., Schefuß, E., Wefer, G., 2014. Pliocene
695 environmental change in West Africa and the onset of strong NE trade winds
696 (ODP Sites 659 and 658). Palaeogeogr. Palaeoclimatol. Palaeoecol. 414, 403–
697 414.
698 Van Baak, C.G.C., 2015. Mediterranean-Paratethys connectivity during the late
699 Miocene to Recent. PhD Thesis Utrecht University.
700 Van Baak, C.G.C., Grothe, A., Richards, K., Stoica, M., Aliyeva, E., Davies, G.R.,
701 Kuiper, K.F., Krijgsman, W., 2019. Flooding of the Caspian Sea at the
702 intensification of Northern Hemisphere Glaciations. Glob. Planet. Change 174,
703 153–163.
704 Van Baak, C.G.C., Vasiliev, I., Stoica, M., Kuiper, K.F., Forte, A.M., Aliyeva, E.,
705 Krijgsman, W., 2013. A magnetostratigraphic time frame for Plio-Pleistocene
706 transgressions in the South Caspian Basin, Azerbaijan. Glob. Planet. Change
707 103, 119–134.
708 Vincent, S.J., Davies, C.E., Richards, K., Aliyeva, E., 2010. Contrasting Pliocene
709 fluvial depositional systems within the rapidly subsiding South Caspian Basin; a
710 case study of the palaeo-Volga and palaeo-Kura river systems in the Surakhany
711 Suite, Upper Productive Series, onshore Azerbaijan. Mar. Pet. Geol. 27, 2079–
712 2106.
713 York, D., 1969. Least squares fitting of a straight line with correlated errors. Earth
714 Planet. Sci. Lett. 5, 320–324.

715

716 Figure and table captions

717

Figure 1. Location of Lokbatan section in Azerbaijan: a) location of the studied sedimentary sequence in global and regional contexts. The black polygon highlighted on the globe (inset top left) shows the location of the regional map. Red rectangle on the regional map indicates the area covered by map b, yellow dot shows the location of the studied section; b) location of the Lokbatan section (yellow dot) and names of sites and geographical features mentioned in the text. Numbered items are 1: Mineral'nyye Vody, 2: Tersko-Sunzhensky/Dagestan foothills, 3: Akchagylian localities of Bashkortostan. Extent of the Caspian Sea at the time of the Plio-Pleistocene transition is shaded blue with thick blue edge, with the possible route of overspill to the Azov region indicated by the blue arrow. Light blue-grey shading indicates the current Caspian drainage while light green indicates areas that now drain to the Black Sea (modified from Van Baak et al., 2019).

Figure 2. a) Lithostratigraphic log of the Akchagylian interval of the Lokbatan section, Azerbaijan, showing the positions of the intercalated ashes (numbered 1 to 9). Stratigraphic levels are correlated with those published by Van Baak et al. (2013); b) benthic oxygen isotope stack of Lisiecki and Raymo (2005). Interglacial periods shaded orange and glacial periods shaded blue (note that this curve is plotted with lower values towards the top); c) Age-depth model of the studied Lokbatan section. The model selected is a linear regression and has been built using Clam (Blaauw, 2010). Model uncertainty is indicated by grey shading. Two of the dates (ash 7 and ash 9) were not incorporated into the age-depth model as they overlap in age with dates from lower stratigraphic levels.

Figure 3. $^{40}Ar/^{39}Ar$ Ideogram (probability distribution plots). Red dots indicate crystals that are not included in the calculation either due to lower K/Ca values or because they are not part of the normal distribution. All information related to each analysis (J-values, ratios and plots) can be found in supplementary material .

Figure 4. Pollen diagram of the studied Lokbatan section. Horizontal axis shows percentage representation of tree pollen types, with all taxa except *Pinus* plotted after recalculation of percentages excluding *Pinus*. *Taxodium* type refers to the pollen grain of the Taxodioideae subfamily (formerly Taxodiaceae). Pollen assemblage zones (PAZ) are marked. A light grey bar indicates barren samples. All horizontal percentage axes are plotted on the same scale unless otherwise indicated. Lithostratigraphic log (left), shows positions of the intercalated ashes (numbered 1 to 9). All raw data and calculations are provided in supplementary material.

Figure 5. Pollen diagram of the studied Lokbatan section. Horizontal axis shows percentage representation of shrub and herb pollen types, terrestrial pollen sum, concentrations of terrestrial pollen (grains per $cm^3 \times 10^3$), and the pollen assemblage zones (PAZ). All taxa are plotted after recalculation of percentages excluding *Pinus*. A light grey bar indicates barren samples. All horizontal percentage axes are plotted on the same scale unless otherwise indicated. Lithostratigraphic log (left), shows positions of the intercalated ashes (numbered 1 to 9). All raw data and calculations are provided in supplementary material.

Figure 6. Pollen diagram of the studied Lokbatan section. Horizontal axis shows percentage representation of pollen types of aquatic vegetation, fern spores, non-pollen palynomorphs (NPP), reworked palynomorphs, PAZ, and the results of the CONISS cluster analysis. All taxa are plotted as a percentage of the terrestrial pollen sum after excluding *Pinus*. A light grey bar indicates barren samples. All horizontal percentage axes are plotted on the same scale unless otherwise indicated. Lithostratigraphic log (left), shows positions of the intercalated ashes (numbered 1 to 9). All raw data and calculations are provided in supplementary material.

Figure 7. Chronology of vegetation change in the South Caspian Sea Basin and global climate changes during the Plio-Pleistocene transition. From top to bottom: a) pollen assemblage zones (PAZ) (Fig. 4, 5 and 6); b) variations in obliquity (angle between the equator and orbital plane), from Laskar et al. (2004); c and d) ratio of arboreal pollen (AP) to non-arboreal pollen (NAP) (=AP/NAP). Both c and d show data points (grey circles joined by dotted line) and a three point moving average (solid lines). Ratio calculation for the green curve (c) included *Pinus* and undifferentiated bisaccate grains while these were excluded for the calculation of the brown curve (d); e) ages and error margins of argon dates obtained from volcanic ashes in the Lokbatan section; f) benthic oxygen isotope stack of Lisiecki and Raymo (2005) showing glacial-interglacial variability (interglacials towards the top). Pale yellow bars illustrate the suggested correlation between our record and the published global records. Volcano icons illustrate the position of volcanic ash layers, with $^{40}Ar/^{39}Ar$ ages shown (where available). Data for AP/NAP curves is provided in supplementary material.

791 Table 1. Summary of $^{40}Ar/^{39}Ar$ biotite ages for this study. Age-depth correlation in

792 Figure 2 was modelled using the ideogram ages. All errors stated represent 2 σ.

793

Table 1. Summary of $^{40}Ar/^{39}Ar$ biotite ages for this study.

Sample Name	Sample level (m)	Material Analyzed	Size Range (μm)	Ideogram [Model] Age (Ma)	MSWD	Inverse Isochron Age (Ma)	MSWD	Total Fusion Age (Ma)
Ash Layer 1	528.80	Biotite	106-150	2.73 ± 0.09	2.01	2.66 ± 0.24	1.29	2.12 ± 0.28
Ash Layer 2	532.00	Biotite	106-150	2.68 ± 0.03	2.56	2.75 ± 0.09	2.68	2.61 ± 0.03
Ash Layer 3	532.60	Biotite	106-150	2.67 ± 0.02	1.30	2.84 ± 0.11	1.29	2.68 ± 0.03
Ash Layer 4	533.00	Biotite	106-150	2.66 ± 0.02	1.76	2.72 ± 0.03	1.75	2.72 ± 0.02
Ash Layer 5	534.40	Biotite	106-150	2.60 ± 0.03	1.31	2.67 ± 0.06	1.41	2.72 ± 0.03
Ash Layer 7	537.80	Biotite	106-150	2.73 ± 0.05	2.78	2.72 ± 0.09	2.12	2.79 ± 0.06
Ash Layer 9	541.20	Biotite	106-150	2.66 ± 0.05	3.51	2.60 ± 0.23	4.02	2.69 ± 0.07

Note: All Ages are at 2-sigma

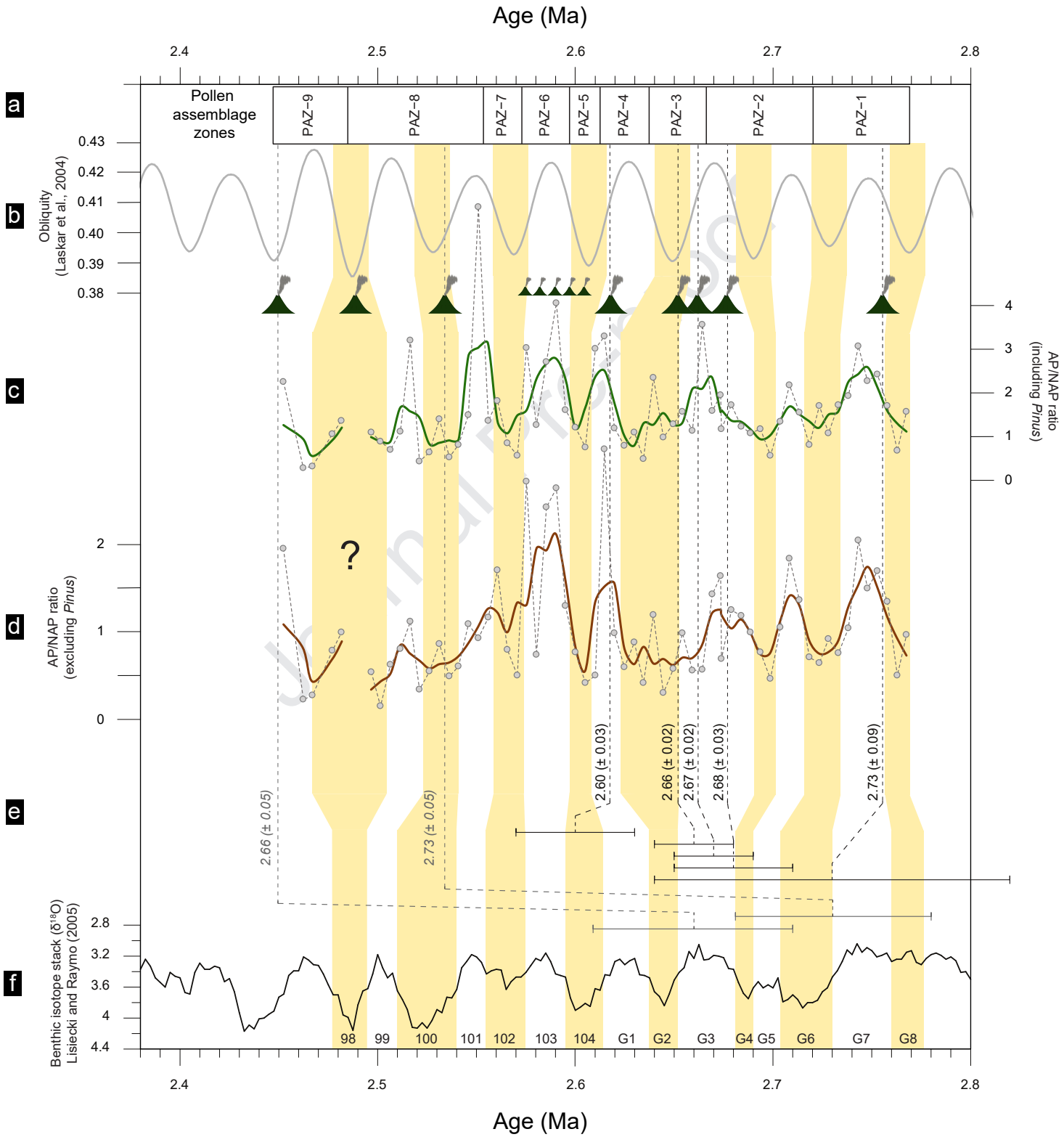
Age (Ma)
2.4
2.5
2.6
2.7
2.8
a
Pollen assemblage zones
PAZ–9
PAZ–8
PAZ–7
PAZ–6
PAZ–5
PAZ–4
PAZ–3
PAZ–2
PAZ–1
b
Obliquity (Laskar et al., 2004)
0.43
0.42
0.41
0.40
0.39
0.38
c
AP/NAP ratio (including Pinus)
4
3
2
1
0
d
AP/NAP ratio (excluding Pinus)
2
1
0
?
e
2.66 (± 0.05)
2.73 (± 0.05)
2.60 (± 0.03)
2.66 (± 0.02)
2.67 (± 0.02)
2.68 (± 0.03)
2.73 (± 0.09)
f
Benthic isotope stack (δ18O) Lisiecki and Raymo (2005)
2.8
3.2
3.6
4
4.4
98
99
100
101
102
103
104
G1
G2
G3
G4
G5
G6
G7
G8
Age (Ma)

Fig. 07

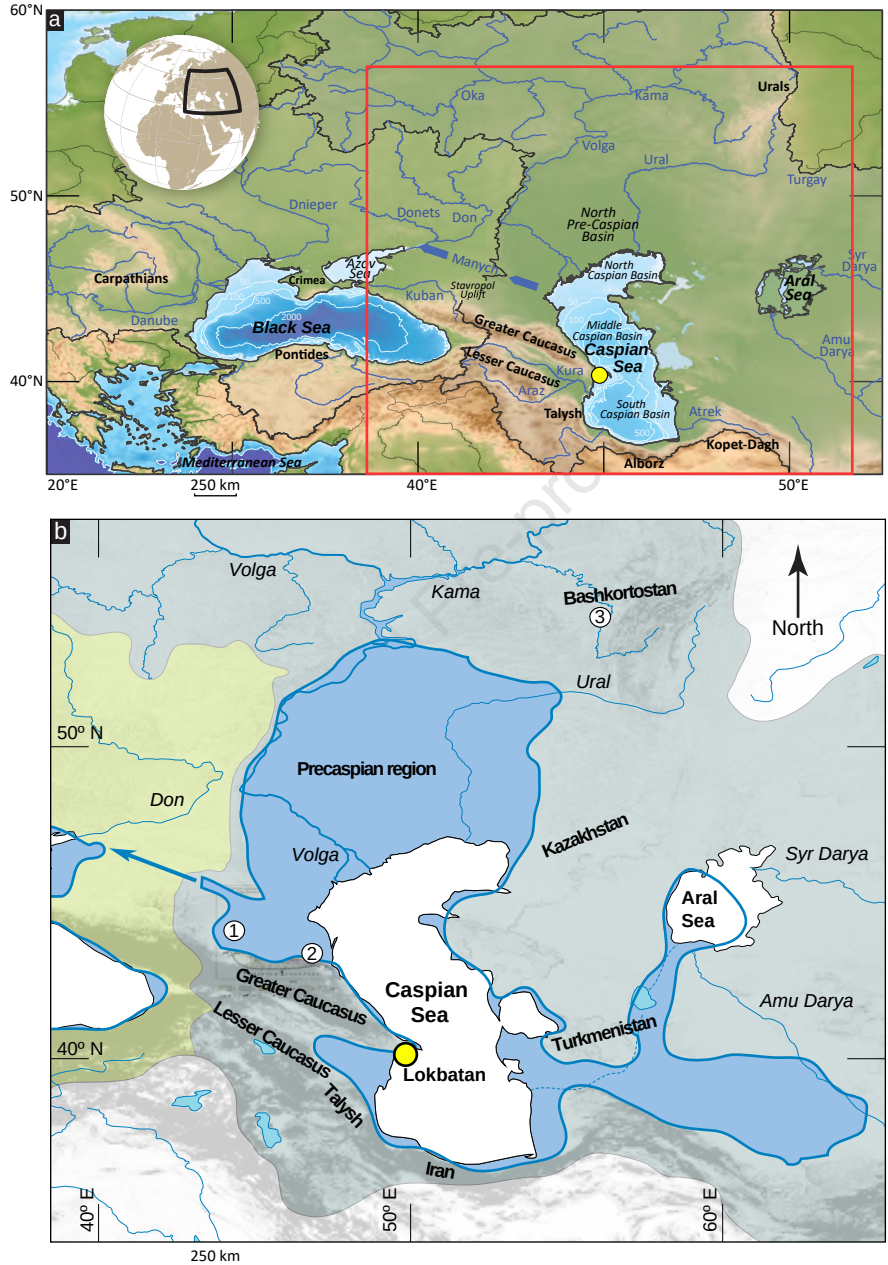
a
60°N
50°N
40°N
20°E
40°E
50°E
250 km
Oka
Kama
Urals
Volga
Ural
Turgay
Dnieper
Donets
Don
North Pre-Caspian Basin
Manych
Azov Sea
Crimea
Carpathians
Kuban
Stavropol Uplift
North Caspian Basin
Aral Sea
Syr Darya
Danube
Black Sea
Pontides
Greater Caucasus
Lesser Caucasus
Middle Caspian Basin
Caspian Sea
Kura
Araz
Amu Darya
Talysh
South Caspian Basin
Atrek
Kopet-Dagh
Alborz
Mediterranean Sea
b
Volga
Kama
Bashkortostan
North
Ural
50º N
Precaspian region
Don
Volga
Kazakhstan
Syr Darya
Aral Sea
Caspian Sea
Greater Caucasus
Lesser Caucasus
Talysh
Lokbatan
Turkmenistan
Amu Darya
40º N
Iran
40º E
50º E
60º E
250 km

Fig. 1

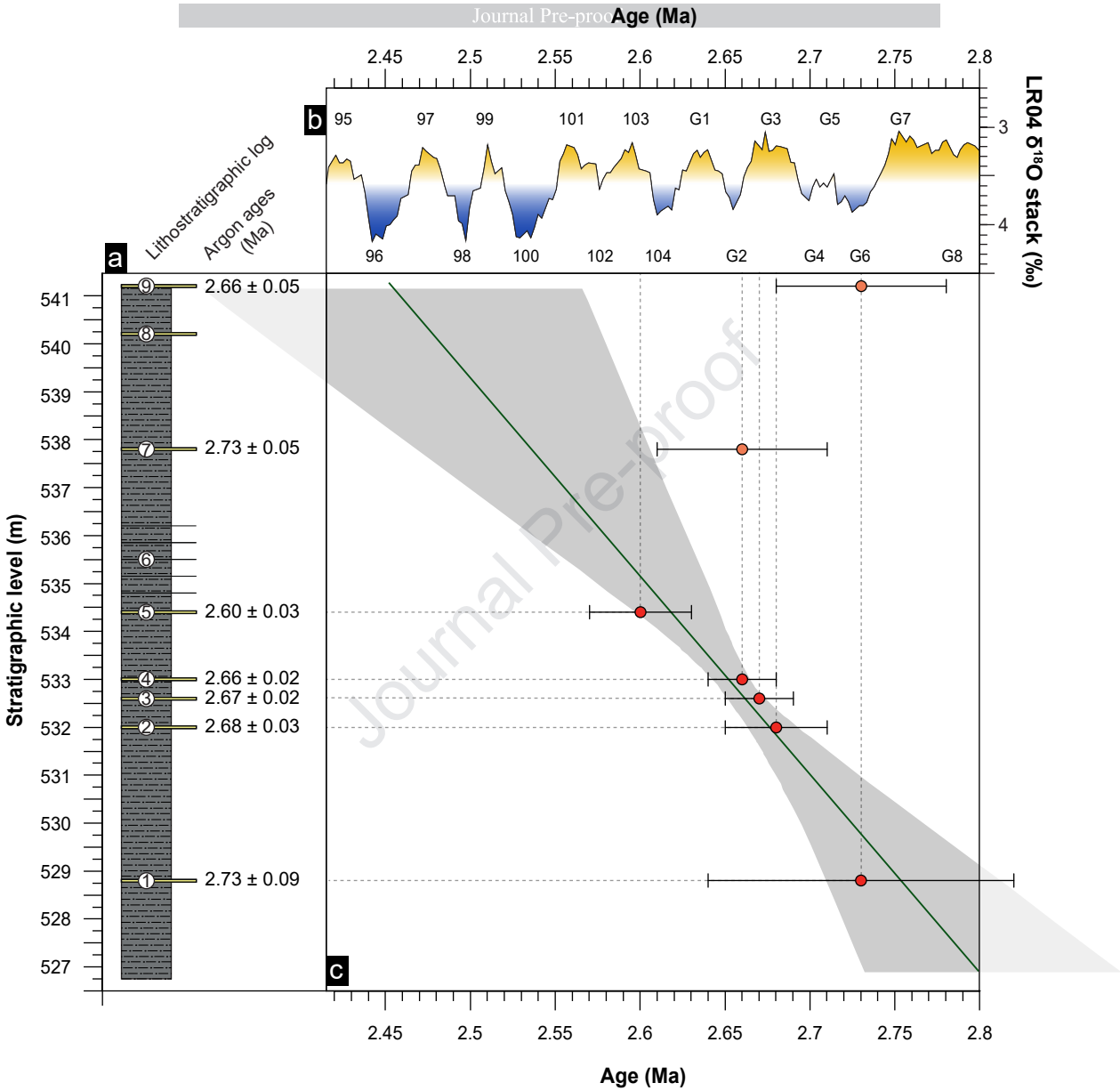

Fig. 02

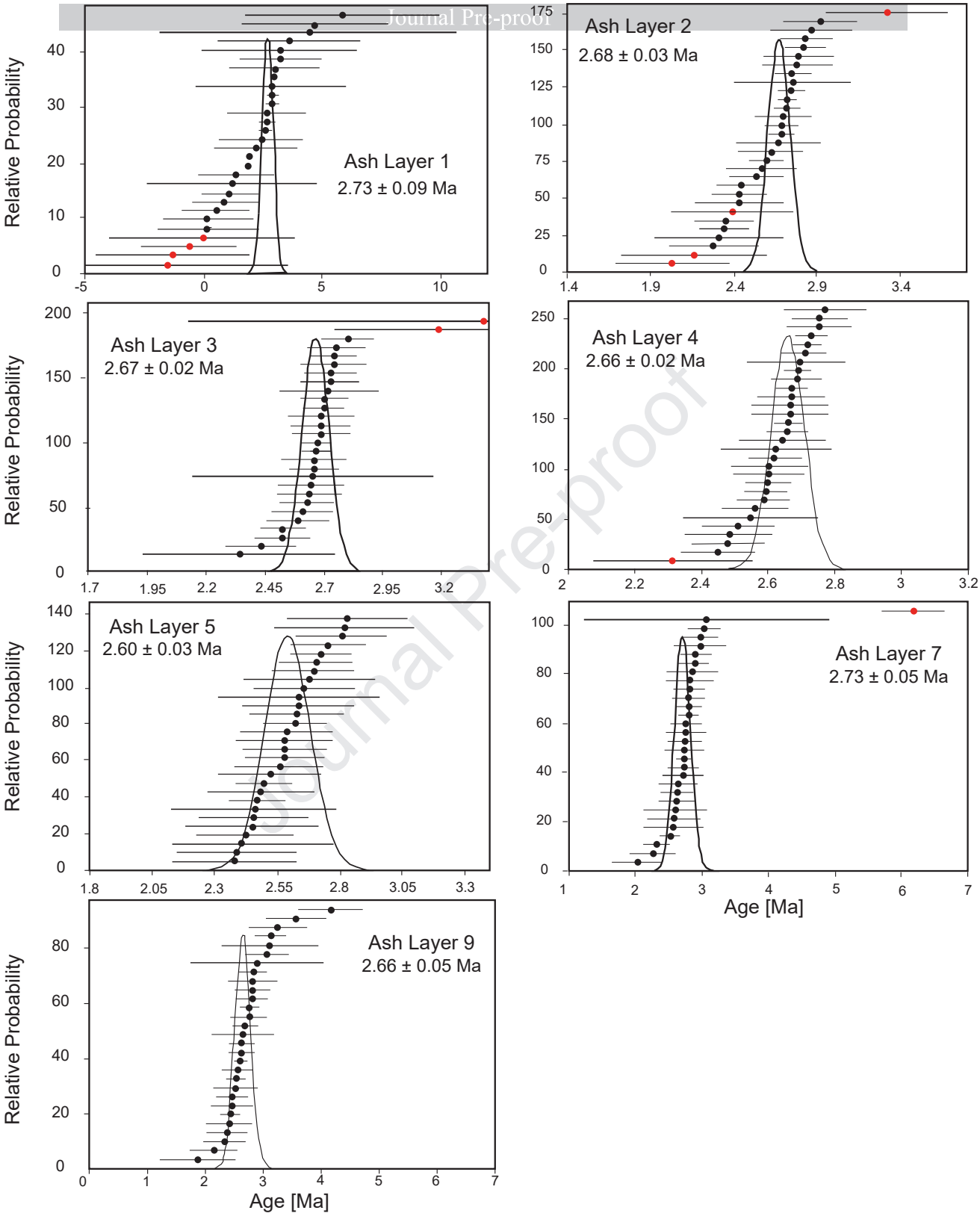

Fig. 03

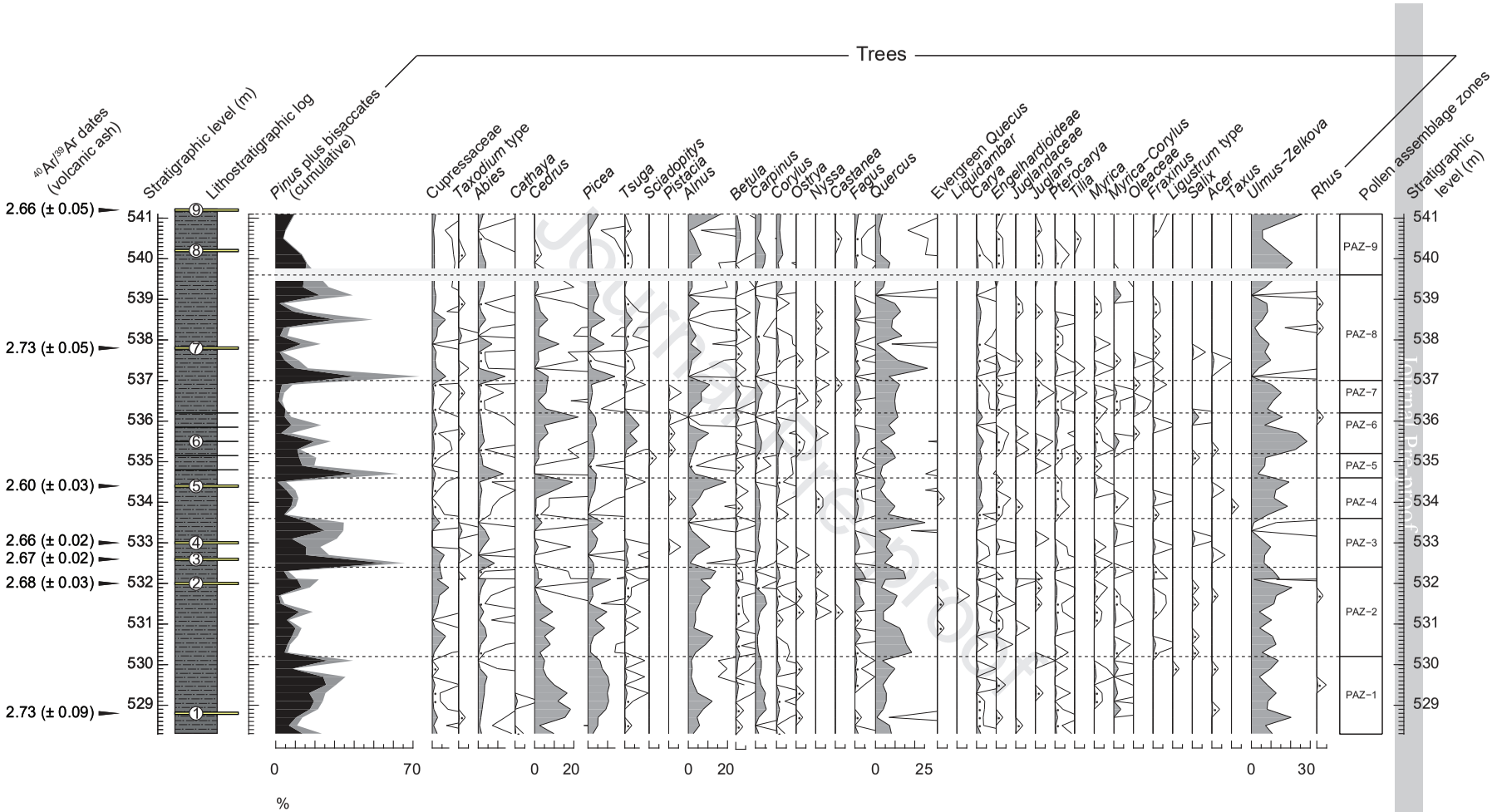
Trees
$^{40}Ar/^{39}Ar$ dates (volcanic ash)
Stratigraphic level (m)
Lithostratigraphic log
Pinus plus bisaccates (cumulative)
Cupressaceae
Taxodium type
Abies
Cathaya
Cedrus
Picea
Tsuga
Sciadopitys
Pistacia
Alnus
Betula
Carpinus
Corylus
Ostrya
Nyssa
Castanea
Fagus
Quercus
Evergreen Quecus
Liquidambar
Carya
Engelhardioideae
Juglandaceae
Juglans
Pterocarya
Tilia
Myrica
Myrica–Corylus
Oleaceae
Fraxinus
Ligustrum type
Salix
Acer
Taxus
Ulmus–Zelkova
Rhus
Pollen assemblage zones
Stratigraphic level (m)
2.66 (± 0.05)
2.73 (± 0.05)
2.60 (± 0.03)
2.66 (± 0.02)
2.67 (± 0.02)
2.68 (± 0.03)
2.73 (± 0.09)
PAZ–9
PAZ–8
PAZ–7
PAZ–6
PAZ–5
PAZ–4
PAZ–3
PAZ–2
PAZ–1
0
70
0
20
0
20
0
25
0
30
%

Fig. 04

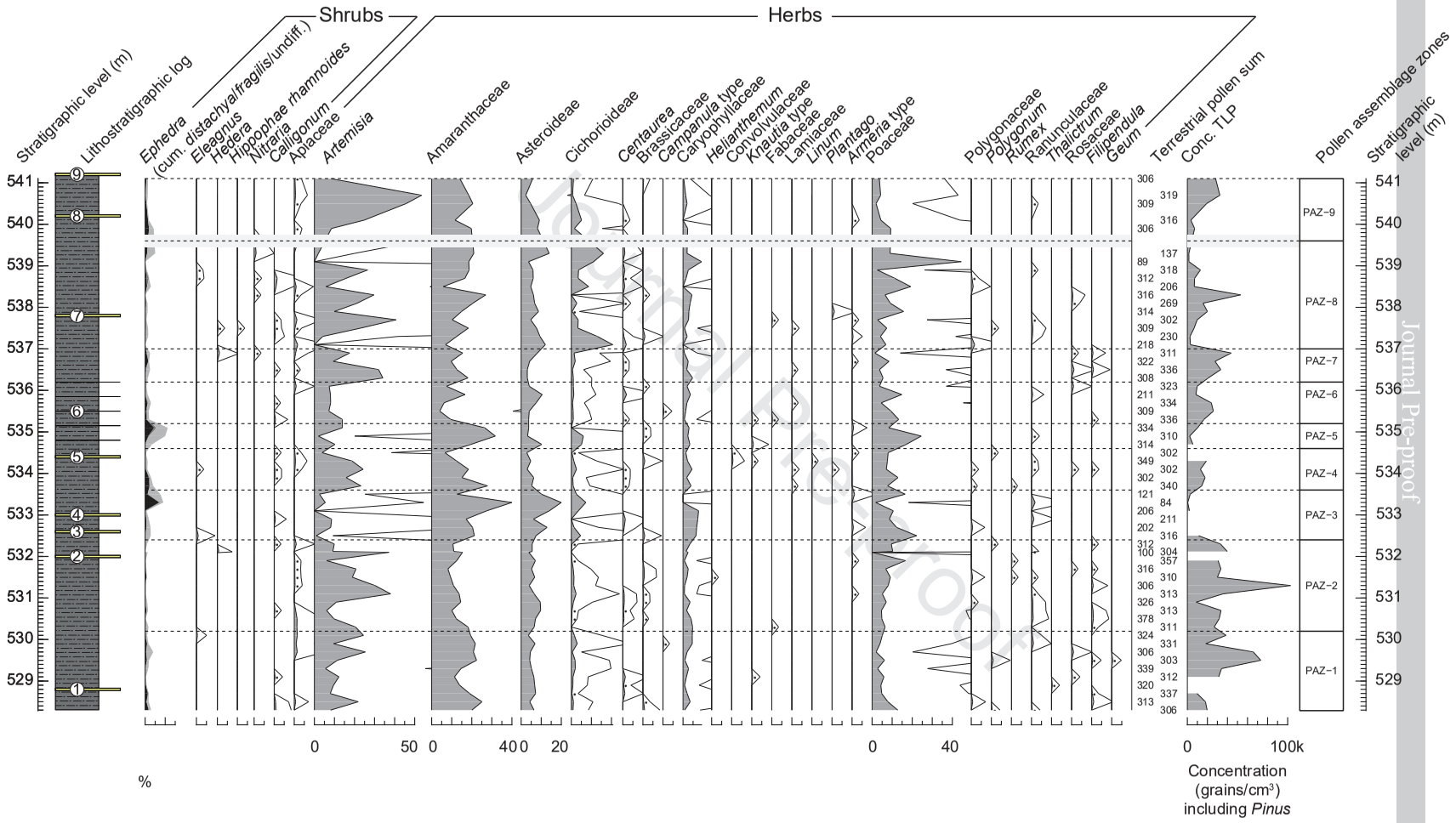
Shrubs
Herbs
Stratigraphic level (m)
Lithostratigraphic log
Ephedra (curn. distachya/fragilis/undiff.)
Eleagnus
Hedera
Hippophae rhamnoides
Nitraria
Caligonum
Aplaceae
Artemisia
Amaranthaceae
Asteroideae
Cichorioideae
Centaurea
Brassicaceae
Campanula type
Caryophyllaceae
Helianthemum
Convolvulaceae
Knautia type
Fabaceae
Lamiaceae
Linum
Plantago
Armeria type
Poaceae
Polygonaceae
Polygonum
Rumex
Ranunculaceae
Thalictrum
Rosaceae
Filipendula
Geum
Terrestrial pollen sum
Conc. TLP
Pollen assemblage zones
Stratigraphic level (m)
PAZ-9
PAZ-8
PAZ-7
PAZ-6
PAZ-5
PAZ-4
PAZ-3
PAZ-2
PAZ-1
%
Concentration (grains/cm³) including Pinus
Journal Pre-proof

Fig. 05

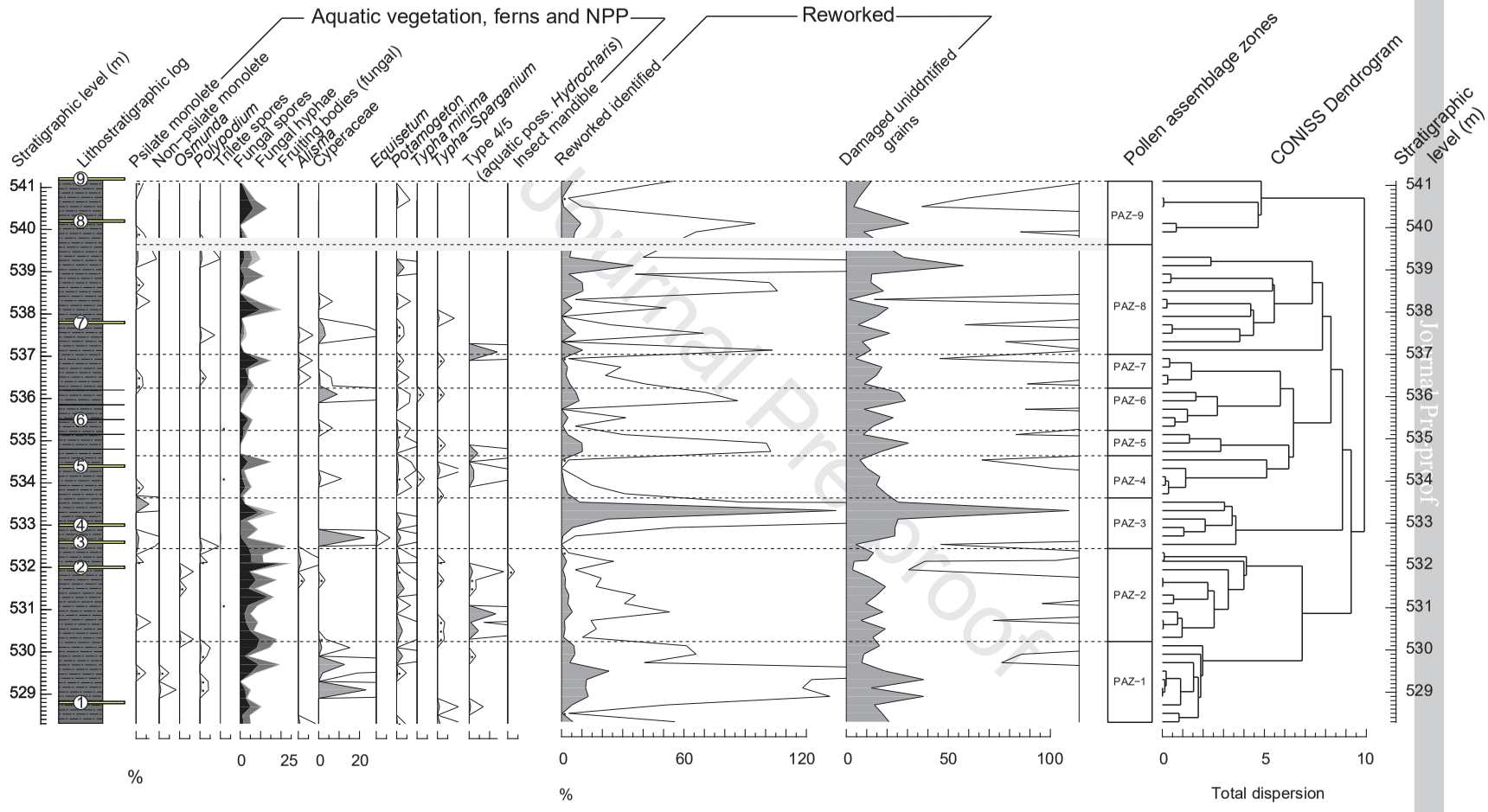

Fig. 06

Vegetation succession and climate change across the Plio-Pleistocene transition in eastern Azerbaijan, central Eurasia (2.77–2.45 Ma)

Highlights

- Plio-Pleistocene vegetation and climate change is studied based on palynological records from eastern Azerbaijan
- Records are deciphered at Milankovitch timescales and correlate with glacial-interglacial cycles MIS G8 to 97 (~2.77–2.45 Ma)
- Caucasus region acted as a refugium for warm-humid forests during the earliest Pleistocene glaciations
- Vegetation response was muted by moisture availability due to Caspian flooding